iScience

CellPress
OPEN ACCESS

Article

Nanoarchitectonics on residual carbon from gasification fine slag upon two step low temperature activation for application in supercapacitors

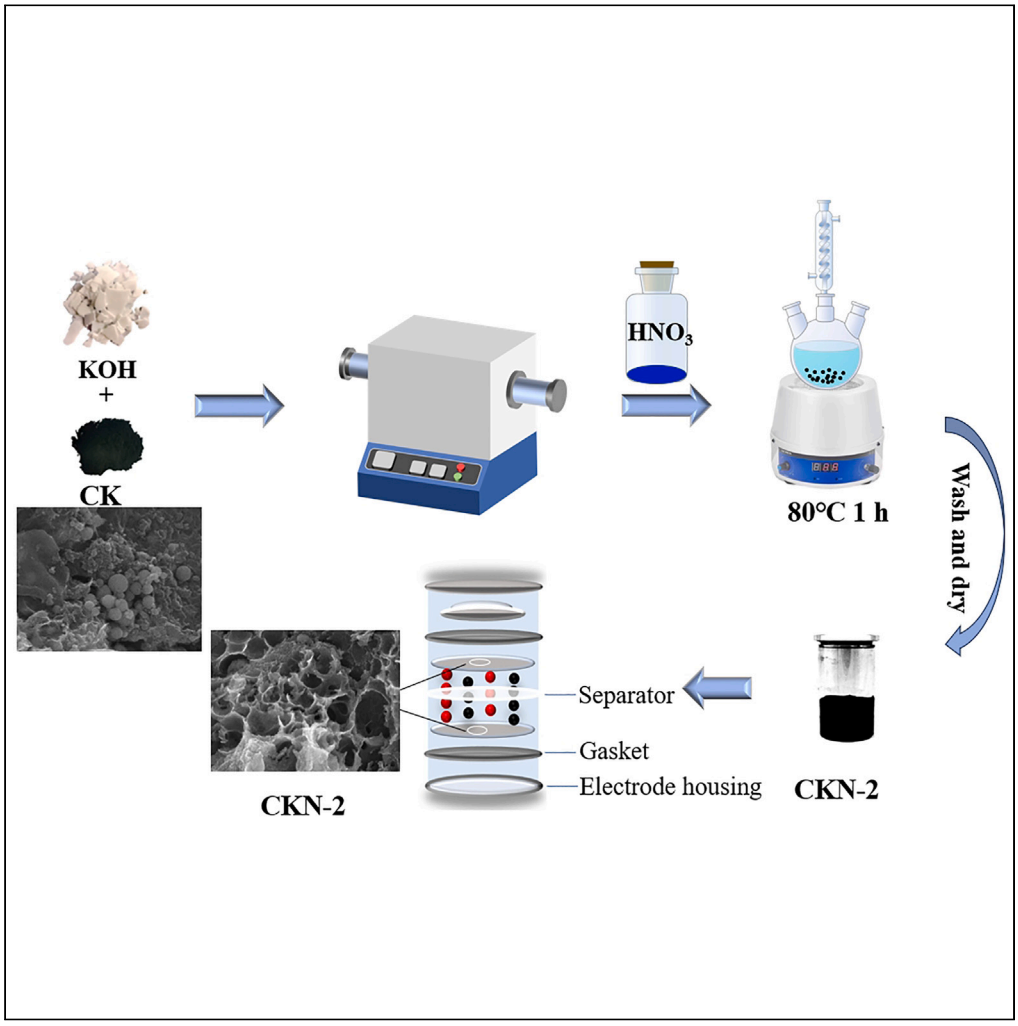

Jiaqi Zhu, Jinling Song, Baobao Han, Jianmin Gao, Zhongyi Liu, Yao Wang, Guoxiang Xin

sjl2010004@imust.edu.cn

Highlights

The carbon electrode materials were prepared by the KOH-HNO_3 low-temperature activation technique using cheap residual carbon from gasification fine slag (CK) as raw materials

The prepared material (CKN-2) which obtained by dry-wet sequential activation at 500°C for 1.5 h at carbon to KOH ratio of 1:2 and further at 80°C for 1 h in 2 mol/L HNO_3 solution

The specific capacitance of CKN-2 reached 142 F/g at a current density of 0.5 A/g

An energy density of 6.80 Wh/kg at a power density of 244.8 W/kg

Zhu et al., iScience 26, 108186
November 17, 2023
https://doi.org/10.1016/j.isci.2023.108186

iScience

CellPress
OPEN ACCESS

Article

Nanoarchitectonics on residual carbon from gasification fine slag upon two step low temperature activation for application in supercapacitors

Jiaqi Zhu,[1] Jinling Song,[1,3,*] Baobao Han,[1] Jianmin Gao,[2] Zhongyi Liu,[2] Yao Wang,[2] and Guoxiang Xin[1]

SUMMARY

In this paper, the carbon electrode materials were prepared by the KOH-HNO_3 low-temperature activation technique using cheap residual carbon from gasification fine slag (CK) as raw materials. The results showed that the prepared material (CKN-2) which obtained by dry-wet sequential activation at 500°C for 1.5 h at carbon to KOH ratio of 1:2 and further at 80°C for 1 h in 2 mol/L HNO_3 solution. The specific capacitance of CKN-2 reached 142 F/g at a current density of 0.5 A/g. CKN-2 was used to assemble a symmetrical (CKN-2//CKN-2) supercapacitor, which exhibited an energy density of 6.80 Wh/kg at a power density of 244.8 W/kg. The CKN-2//CKN-2 capacitor was tested for stability after 10,000 cycles, with a capacitance retention rate of 97%. These results demonstrate that residual carbon from gasification fine slag can be effectively used to produce high-performance carbon electrode materials for supercapacitors using the KOH-HNO_3 low-temperature sequential co-activation technique.

INTRODUCTION

Coal remains a dominant source of traditional energy and is commonly utilized through coal gasification technology. However, this process generates a significant amount of gasification residue, also known as gasification slag. To maximize the utilization of this byproduct, the slag can be purified to form high-quality carbon, which has a wide range of applications. One notable application is as electrode material for supercapacitors, which are high-performance energy storage devices capable of rapid charging and discharging. Compared to lithium batteries, supercapacitors exhibit a significantly longer cycle life, capable of enduring tens of thousands of charge/discharge cycles without significant capacity or performance degradation. They maintain superior performance at high temperatures, unlike lithium batteries that are susceptible to damage under such conditions. Compared to fuel cells, supercapacitors do not need complex fuel supply systems or oxidizers, resulting in lower maintenance requirements. Additionally, supercapacitors are environmental-friendly as they do not contain heavy metals or hazardous substances and can be easily recycled and reused, minimizing their environmental pollution.[1–3]

Based on the aforementioned advantages, supercapacitors have garnered significant attention from academia and industry in recent years due to their high energy density and cycling stability.[4] The electrode materials are the heart of these supercapacitors, with carbon materials being the most common due to their large specific surface area, good electrical conductivity, and relatively low cost.[5] Consequently, they have become the most commercially successful materials.[6] The large-scale deployment of clean energy has made the development of clean-energy carbon electrode materials a research hotspot around the world.[7]

Residual carbon from gasification fine slag is a common by-product or waste material that often requires treatment and disposal. Through low-temperature activation, these wastes can be converted into useful materials or energy. This conversion process helps to improve resource utilization and reduce environmental pollution. Activated samples may have good electrochemical properties such as high specific surface area and electrical conductivity. These properties make them ideal materials for energy storage and conversion devices such as electrochemical supercapacitors, lithium-ion batteries, or fuel cells. Activated samples with abundant surface functional groups and pore structures are ideal candidates for catalysts or adsorbents. These materials can be applied in catalytic reactions, gas or liquid adsorption, and wastewater treatment, contributing to advances in chemistry and the environment. The conversion of residual carbon from gasification fine slag into useful products has circular economy and sustainable development implications. Through the development of activation technologies, it is possible to convert waste into high value-added products, reducing dependence on virgin resources, waste emissions, and environmental impacts. This contributes to a sustainable social and economic system. From a broader scientific and technological perspective, exploring and optimizing the low-temperature activation steps of residual carbon from gasification

[1]School of Materials and Metallurgy, Inner Mongolia University of Science and Technology, Baotou, Inner Mongolia 014010, China
[2]Inner Mongolia Bdsd Chemical Co, Ltd, Inner Mongolia 017004, China
[3]Lead contact
*Correspondence: sjl2010004@imust.edu.cn
https://doi.org/10.1016/j.isci.2023.108186

fine slag is a challenging and interesting research topic. This work contributes to the advancement of cutting-edge knowledge and technology in the fields of materials science, energy technology, and environmental engineering. Thus, the utilization of gasification slag to produce nanoporous carbon for supercapacitor electrodes is a sustainable and practical approach that can help to reduce waste and provide a clean energy source. This can contribute to the development of a circular economy and promote environmental sustainability in the energy fields.

The majority of current nanoporous carbon electrode materials are produced using biomass char as a precursor through high-temperature activation charring. Several studies have investigated the use of various raw materials to produce carbon electrode materials. For instance, Akdemir et al.[8] utilized biomass char as a raw material and obtained a material with a specific capacitance value of 89 F/g at a current density of 1 A/g after high-temperature activation with KOH. Awitdrus et al.[9] employed pineapple honey peel as a raw material and activated it at 600°C. Alberto et al.[10] used waste coffee grounds as the charcoal material and achieved a specific capacitance value of 84 F/g at a current density of 1 A/g after chemical activation. Shrestha et al.[11] used wood chips as the raw material and obtained a specific capacitance value of 42.2 F/g at a current density of 1 A/g after KOH activation. Yaglikci et al.[12] utilized waste tea as a raw material and achieved a specific capacitance value of 101 F/g at a current density of 1 A/g after using $Na_2S_2O_3$-$5H_2O$ as an activator at 800°C. Sharma et al.[13] conducted chemical activation using wheat straw and found that the acid-activated wheat straw had a specific capacitance of 162 F/g, while the alkali-activated wheat straw had a specific capacitance of 106 F/g due to different surface functional groups in the respective carbon frameworks. Mahfoz et al.[14] prepared a novel submicron-nanocarbon from date leaves through simple pyrolysis and ball milling, which exhibited a specific capacitance of 107 F/g with 92% capacitance retention after 10,000 charge/discharge cycles.

Besides aforementioned single activation, several activation methods were applied to the preparation of carbon electrode materials. Zhang et al.[15] developed a carbon material with a specific capacitance of 129 F/g using snow lotus as a raw material through two activation methods KOH-chemical activation and mixed molten salt synthesis. Qu et al.[16] prepared a carbon material modified with porous carbon through H_3PO_4 activation and nitrogen and phosphorus co-doping using rice husk as a carbon source, achieving a specific capacitance of 130 F/g at a current density of 0.5 A/g. Gong et al.[17] utilized spiral carbon nanofibers as the raw material and prepared material with a specific capacitance of 143.6 F/g at a current density of 1A/g through a two-step method involving HNO_3 treatment and a modified Hummers' method to improve surface properties. Dat et al.[18] employed expired milk for hydrothermal carbonization and continuous KOH-H_3PO_4 activation to obtain a carbon material with a modified specific capacitance of 186.3 F/g.

After comparative analysis, it can be concluded that KOH can react with some inorganic minerals in the residual carbon of gasification slag to increase the carbon content of the material, and HNO_3 activation can effectively introduce oxygen-containing functional groups in the carbon skeleton to improve the hydrophilicity of the material. In addition, both KOH and HNO_3 activation can change the pore structure of the material and increase the content of micropores and mesopores. However, in a single activation process, the activation degree is relatively low due to the limitation of the reaction degree between the carbon material and the activator. Borrowing from the aforementioned results, if KOH is firstly utilized to remove the inorganic minerals on the carbon surface, more carbon surface will be exposed to provide more contact sites for the subsequent activation. And then HNO_3 activation is utilized to modulate the pore structure on the one hand, and to introduce the oxygen-containing functional groups on the carbon skeleton on the other hand, so that the contents of the micropores, mesopores, and oxygen-containing functional groups can be increased, and the specific surface area of the material can be increased, which can lead to the enhancement of electrochemical performances.

To develop new energy storage devices like supercapacitors, carbon electrode materials with low-cost and high specific surface area are very urgent needs. However, most carbon electrode materials are currently produced by high-temperature activation (>700°C) using biomass as raw materials. Therefore, in this paper, the sequence of KOH-HNO_3 was chosen to jointly activate the residual carbon from gasification fine slag. A carbon electrode material with superior performance was produced using a two-step, low-temperature activation method of KOH-HNO_3. The raw material was the residual carbon from gasification fine slag, which was separated and extracted using gravitational separation technology by a company located in Inner Mongolia Autonomous Region, China. The composition and structure of the material were thoroughly characterized, and its electrochemical properties were systematically evaluated.

Material analysis

Figures 1A and 1B depict the microscopic morphology of residual carbon (CK), which is the residual carbon from the gasification slag. CK consists of a lamellar structure formed by nanoscale carbon (80–300 nm) and micron-sized spherical inorganic minerals that melted at high temperatures during the gasification process. In contrast, Figures 1C and 1D show the microscopic morphology of carbon residue from gasification slag treated with 2 mol/L KOH (CK-2), where the spherical inorganic minerals significantly disappeared. CK-2 exhibits nano-flocculated porous carbon structure with a small interlayer distance (60–150 nm), which is likely due to the melting of KOH during 360°C–380°C. During this temperature range, KOH chemically reacts with carbon and releases gases such as H_2, CO, and CO_2 in real-time to create pores.[19] Alternatively, unstable amorphous carbon can also be eroded by KOH to form pores, thereby increasing the specific surface area of the material and providing sites and channels for charge storage and transport.[20]

Figures 1E and 1F illustrate the microscopic morphology of carbon residue from gasification slag treated with 2 mol/L HNO_3 (CN-2), where the carbon layer is thinner (20–70 nm) and less agglomerated. The presence of spherical inorganic minerals in CN-2 suggests that HNO_3 can not effectively remove these minerals. Figures 1G and 1H display the microscopic morphology of carbon residue from gasification slag treated with 2 mol/L KOH and 2 mol/L HNO_3 (CKN-2), which shows that after co-activation with KOH and HNO_3, the material is composed of nanoscale carbon in a lamellar structure (8–20 nm) display fluffy architecture with hierarchical porosity.[21] This nanoporous carbon lamellar

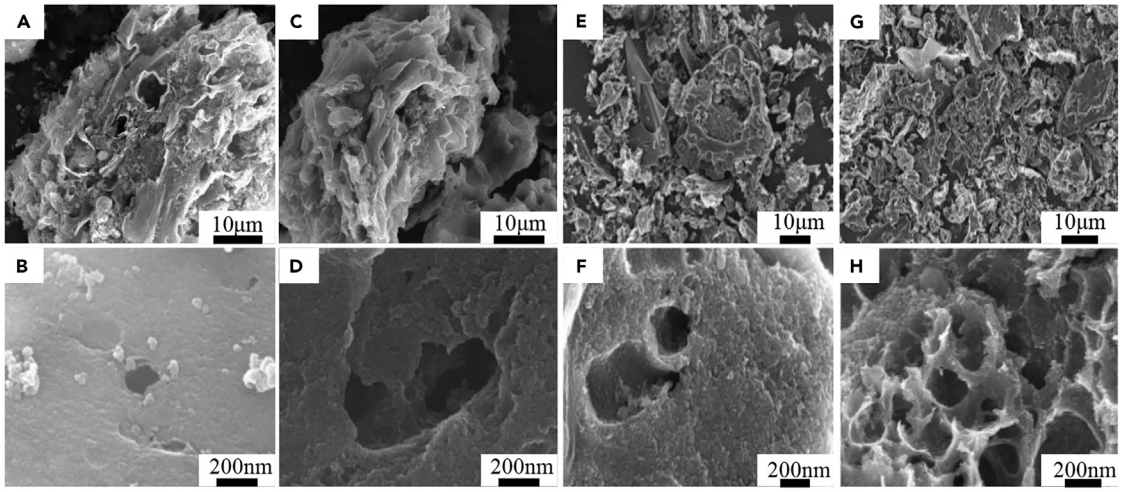

Figure 1. SEM images

SEM images (A and B) CK, (C and D) CK-2, (E and F) CN-2, (G and H) CKN-2.

structure is highly conducive to electrochemical reactions, ion storage, and transport.[22] The disappearance of spherical inorganic minerals indicates that KOH-HNO_3 activation allows for better removal of inorganic minerals from the material.

Figure 2A shows the XRF test results of CK, CK-2, CN-2, and CKN-2. It is evident that CK contains a higher amount of inorganic minerals, and the content of inorganic minerals decreases after KOH activation. However, HNO_3 activation does not affect the content of inorganic minerals, and after KOH-HNO_3 activation, the content of inorganic minerals is further reduced. The removal of inorganic minerals is beneficial for improving electrochemical performance of the material.

Figure 2B shows the XRD patterns of CK, CK-2, CN-2, and CKN-2, with each sample exhibiting a broad characteristic peak at $2\theta = 22°$, corresponding to the diffraction of the graphite (002) surface.[22] The FWHMs of the CKN-2 material are found to be larger than those of CK, CK-2, and CN-2, indicating an increase in defects and amorphous carbon of the material after KOH-HNO_3 activation. The peak at $2\theta = 44°$ for each sample appears to be insignificant, indicating that there is no tendency for graphitization in the activated material. The absence of characteristic peaks for SiO_2 in CK-2 and CKN-2 is evident from the plots and is attributed to the reaction of KOH with SiO_2.[23]

Figure 2C shows the TG curves of the four samples. The weight loss of the materials is not significant at 0°C–500°C, which is due to the volatilization of moisture, decomposition of the active carbon and surface functional groups. During 500°C–700°C, the carbon decomposition result in a weight loss of approximately 58% for CK, 75% for CK-2, 65% for CN-2, and 76% for CKN-2. The relative carbon content in each sample is initially determined by the weight loss rate. After 700°C, the weights of the CK, CK-2, CN-2, and CKN-2 are essentially constant, with residues of approximately 43%, 20%, 32%, and 15%, respectively. These residues mainly consist of inorganic minerals and incombustible carbon. By comparing the aforementioned data, it is apparent that the CKN-2 material has less combustion residue than the other samples, indicating that the CKN-2 material has a higher content of carbon due to the co-activation of KOH-HNO_3. Additionally, the DTG curve in Figure 2D shows that the weight of CKN-2 material lose earlier than those of the other samples, probably due to the activation of KOH-HNO_3 resulting in a loose and porous surface that is more susceptible to thermal decomposition. This result was consistent with the SEM and XRD results.

Figure 2E shows the N_2 adsorption-desorption isotherms for the four samples. At a relative pressure $P/P_0 < 0.1$, several materials exhibit a significant increase in absorption compared to CK, indicating that activation increases the pore capacity of the material. In the range of P/P_0 of 0.42–0.98, the adsorption-desorption isotherms of several materials show a significant hysteresis loop represented type IV (IUPAC), which indicates the presence of mesopores.[24] Figure 3F displays the pore size distribution profiles of the four samples. It is evident that the four materials contained both micropores and mesopores. They were typical nanoporous materials. Micropores might be generated from the intercalation effect of K. The mesopore content of the CKN-2 material is significantly higher than that of the other materials, as shown in the inset of Figure 2F. Specific data on the pore structures of CK, CK-2, CN-2, and CKN-2 are presented in Table 1. The results indicate that, on the one hand, KOH-HNO_3 activation increased the specific surface area of the materials, with CKN-2 having the largest specific surface area of 625 m^2/g. On the other hand, KOH-HNO_3 activation also increased the pore volume and pore size of the materials, with the average pore size (4.690 nm) and mesopore volume (0.495 cm^3/g) of CKN-2 being higher than those of the other materials. This suggests that the activation of HNO_3 increases the number of micropores and mesopores and significantly improves the pore structure. The high specific surface area and high content of mesopores can supply better charge storage sites and ion transport channels, providing structural conditions for improving electrochemical properties.[25]

Figure 2G illustrates the Raman total spectrum of the four samples. The peak intensity ratio (I_D/I_G) of the D and G peaks is a crucial parameter for characterizing the graphitization of carbon materials. The larger ratio indicates a material with more defects, consisting mainly of amorphous carbon and more sp^3 hybridized phases. As shown in the figure, a broad D-peak representing disordered defective carbon

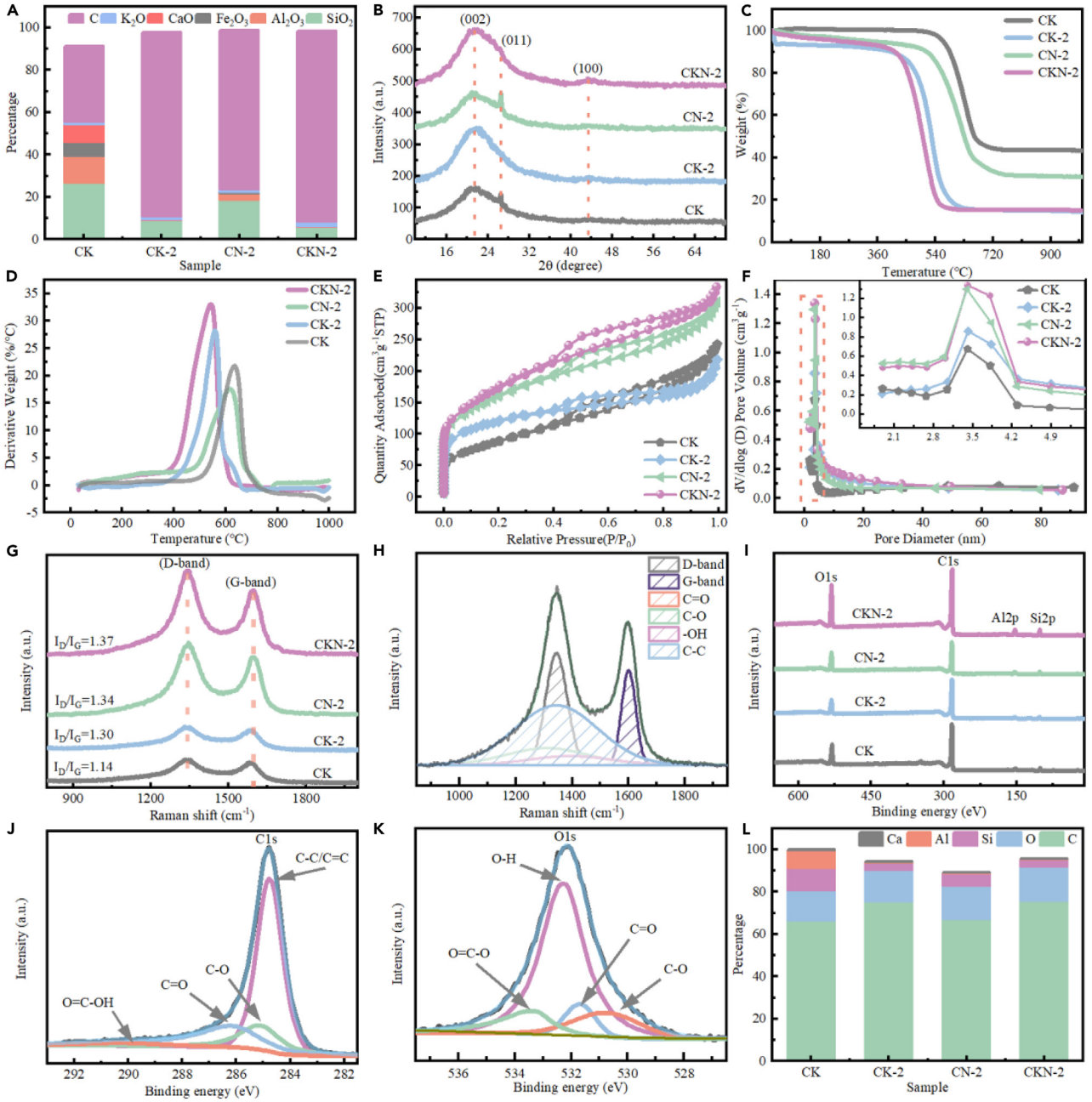

Figure 2. Structural characterisation

CK、CK-2、CN-2, and CKN-2: (A) XRF pattern, (B) XRD pattern, (C) TG curves, (D) DTG curves, (E) N_2 adsorption-desorption isotherms, (F) Pore size distribution, (G) Raman full spectrum, (H) Deconvoluted typical responses of CKN-2, (I) XPS survey pattern, (J) C1s XPS plot of CKN-2, (K) O1s XPS plot of CKN-2, (L) Relative content of elements.

appears near 1,350 cm^{-1} for each sample. A broad G-peak is visible at 1,580 cm^{-1}, which exhibits tangential stretching vibrations of the graphitized carbon atoms. The I_D/I_G of CKN-2 is significantly larger than that of the other materials, indicating that KOH-HNO_3 activation has a greater effect on the structure of the material, and the CKN-2 material has the largest I_D/I_G ratio of 1.37, indicating a relatively high number of defects on the surface of the material.

Figure 2H displays a Gaussian fit splitting spectrum of CKN-2, where the main bands of CKN-2 were Gaussian-fitted to six peaks, including a D peak at 1,350 cm^{-1} and a G peak at 1,580 cm^{-1}. In terms of graphitization, the G peak is very close to 1,600 cm^{-1}, indicating a low degree of graphitization in the sample. The characteristic peak for -OH is at 1,450 cm^{-1}, while the peak for C-C is at 1,200 cm^{-1}. The peaks at 1,250 cm^{-1} and 1,650 cm^{-1} correspond to the C-O and C=O characteristic peaks, respectively.[26] The relative contents of different structures

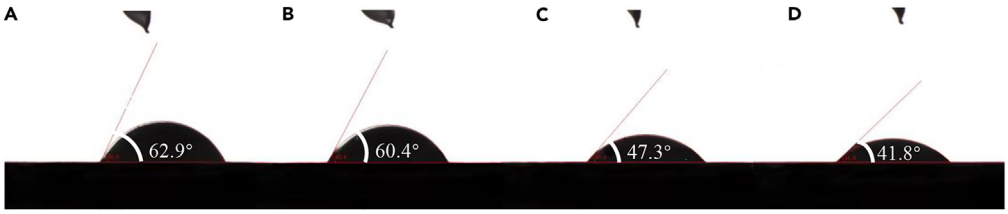

Figure 3. Water contact angle
Water contact angle: (A) CK, (B) CK-2, (C) CN-2, (D) CKN-2.

in CK-2, CN-2, and CKN-2 materials were obtained by calculating the peak areas corresponding to each type of structure, as shown in Table 2. The percentage of oxygen-containing structures in CN-2 is 21.6%, indicating that HNO_3 activation can significantly increase the content of oxygen-containing functional groups. The presence of 26% of oxygen-containing structures in CKN-2 demonstrates that KOH-HNO_3 activation could further increase the content of oxygen-containing functional groups.

Figure 2I shows the total XPS spectra of the four samples, indicating that the samples contain mainly elemental compositions of C, O, Al, and Si. The fine spectral fractionation of C1s of CKN-2 is shown in Figure 2J, including C-C/C=C (284.8 eV), C=O (286.4 eV), C-O (285.4 eV), and O=C-OH (289.1 eV). Figure 2K displays the fine spectral splitting of the O1s of CKN-2, including C-O (531 eV), C=O (531.3 eV), O-H (531.9 eV), and O=C-O (533.3 eV).[30] Figure 2L shows the elemental content of the four samples. It is evident that the C content of CK-2 increases, while the Si, Al, and Ca content decreases, indicating that KOH activation significantly reduces the inorganic mineral content. The O content of CN-2 increases, indicating that HNO_3 activation increases the oxygen-containing functional groups on the surface of the material. The C and O content of CKN-2 increases, while the Si, Al, and Ca content decreases. This indicates that the decrease in inorganic minerals and the increase in oxygen-containing functional groups in the material favor the electrochemical properties, thanks to the synergistic effect of KOH and HNO_3.

The hydrophilicity of electrode material is directly related to its electrochemical properties in an aqueous electrolyte. The water contact angle test provides a visual representation of the hydrophilicity of the material. Figure 3 shows the water contact angle test of the four materials. As shown in the figure, the WCA value of CK is 62.9°, and the WCA value of CK-2 is 60.4°. The WCA of CN-2 reduced to 47.3°, indicating an increase in the hydrophilicity of CN-2 due to the increase in hydrophilic oxygen-containing functional groups on the surface of CN-2 as a result of HNO_3 activation. The combined activation of KOH and HNO_3 resulting in an increase in hydrophilic oxygen-containing functional groups on the surface of the material led to a reduction in the WCA value of 41.8° for the CKN-2 material. It can be demonstrated that the higher number of oxygen-containing functional groups in the CKN-2 material improves the wettability of the material and facilitates the infiltration of electrolyte ions on the surface of the carbon material, which can increase the specific capacitance of the material.[31] These results further validate the results obtained through Raman, XPS, and FT-IR tests from a macroscopic point of view.

On the one hand, KOH activation can significantly improve the pore size distribution of the material, giving it a nanoporous structure, and the high content of mesopores provides a favorable transport channel for electrolyte ions. It also reduces the content of inorganic minerals in the material, providing more contact sites for electrolyte ions. On the other hand, HNO_3 activation can increase the oxygen-containing functional groups on the surface of the material, improving the wettability of the material, which is conducive to the wettability of electrolyte ions on the surface of the carbon material. The co-activation of KOH-HNO_3 can make full use of the characteristics of KOH and HNO_3 to improve the pore size distribution of the material, increase the specific surface area, and the content of oxygen-containing functional groups. The KOH-HNO_3 sequential combined activation approach is more conducive to the electrochemical reaction, providing a better environment for charge storage and ion transport, ultimately leading to improved electrochemical properties of the material.

Electrochemical analysis

The electrochemical performance of CK, CK-2, CN-2, and CKN-2 was evaluated in a three-electrode system, and the results are presented in Figure 4. Figure 4A shows the CV curves of the four materials at a scan rate of 20 mV/s. The rectangular shape of the CV curves for samples CK, CK-2, and CN-2 is more pronounced, indicating that these materials provide bilayer capacitance. In contrast, the CV curve of CKN-2 shows a roughly rectangular trend and a Faraday peak, probably due to the increase in oxygen-containing functional groups on the surface of the material resulting from the activation of KOH-HNO_3. The redox reaction (pseudocapacitance) of these functional groups increases the specific capacitance of the material.[32] This indicates that the CKN-2 material can provide most of the bilayer capacitance and less of the

Table 1. The pore structure data of CK、CK-2、CN-2 and CKN-2

Sample	$S_{BET}(m^2/g)$	$V_{total}(cm^3/g)$	$V_{meso}(cm^3/g)$	$V_{meso}/V_t(\%)$	$D_{ava}(nm)$
CK	319	0.372	0.252	67.742	3.434
CK-2	573	0.420	0.294	70.000	4.774
CN-2	619	0.585	0.482	82.393	4.386
CKN-2	625	0.595	0.495	83.193	4.690

Table 2. Relative content of CK-2、CN-2 and CKN-2 surface structure

Sample	C-C(%)	C=O(%)	C-O(%)	-OH(%)	D-band(%)	G-band(%)
CK-2	49.9	0.1	8.4	8.4	23.5	11.7
CN-2	48.9	0.7	13.6	7.3	23.6	13.1
CKN-2	47.2	1.5	19	5.5	28.6	13.3

pseudocapacitance. Moreover, the CV curve of the CKN-2 material has the largest area, indicating that the CKN-2 material has a more excellent specific capacitance.

Figure 4B shows the GCD curves for CK-2, CN-2, and CKN-2 at a current density of 0.5 A/g. Both CK-2 and CN-2 exhibit an isosceles triangle shape, indicating a double-layer capacitance. The GCD curve for CKN-2 shows a "trailing" shape, which is close to an isosceles triangle, indicating that CKN-2 has a certain pseudocapacitance, consistent with the CV test results. Through calculating according to Equation 4, the specific capacitance values of CK, CK-2, CN-2, and CKN-2 are 35 F/g, 86 F/g, 97 F/g, and 142 F/g, respectively. The result indicates that the specific capacitance increases nearly three times after KOH-HNO_3 activation, suggesting that the nanoporous structure and oxygen-containing functional groups contribute significantly to the electrochemical performance.[33] Table 3 compared to previous electrode materials, the specific capacitance value of CKN-2 is found to be comparable to, and in some cases exceeded, that of biomass carbon electrode materials. Moreover, the KOH-HNO_3 sequential co-activation method offers an effective means of recycling residual carbon from gasification slag, which boasts high yield and low cost relative to other biomass and nanocarbon materials. As such, this approach presents significant potential for generating high-value products from this abundant and economically viable resource.

In Figure 4C, the EIS profiles of the four materials show that CKN-2 has a curve inclination close to 90° in the low-frequency region, indicating ideal specific capacitance properties and low ion diffusion and migration equivalent series resistance. In the high-frequency region, the smaller the semicircle diameter, the lower the charge transfer resistance. After activation, All of the materials have relatively low resistance (<1 Ω). Due to the low resistance of CKN-2, its abundant micro- and mesopores can provide transport channels for electrolyte ions, accelerating electrochemical reactions.[34]

Figure 4D presents the CV curves of CKN-2 at different scan rates. It can be observed that redox peaks still appear on the material surface as the scan rate increases, indicating that the increased capacitance is due to the formation of oxygen-containing functional groups on the material surface after the HNO_3 treatment. The subsequent redox reaction not only improves wettability but also the pseudocapacitance.[35]

$$-C-OH \rightarrow -C=O + H^+ + e^- \quad \text{(Equation 1)}$$

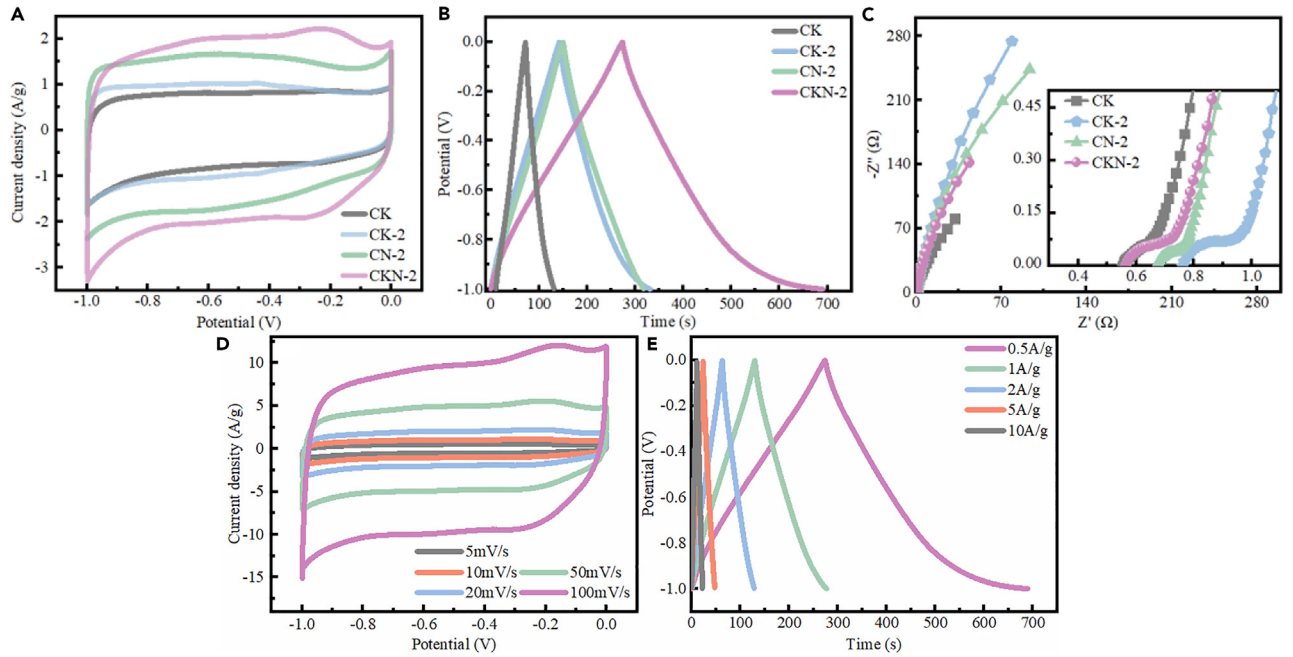

Figure 4. Electrochemical characterisation

Electrochemical performances of CK、CK-2、CN-2, and CKN-2 in a three-electrode system: (A) CV curves at 20 mV/s, (B) GCD curves at 0.5 A/g, (C) EIS curves, (D) CV curves of CKN-2 at different scan rates, (E) GCD curves of CKN-2 at different current densities.

Table 3. Comparison of specific capacitance of recently reported carbon electrode materials

Materials	Activation method	Specific capacitance (F/g)	Vintage	Reference
AC-800	KOH two-step activation	100	2020	Thilageshwaran et al.[27]
SAK	KOH- mixed molten salt	129	2022	Zhang et al.[15]
AC/MWCNTs	KOH-Na_2SO_4	147	2020	Mandal et al.[28]
PK800M	HNO_3-H_2SO_4	182	2022	Punon et al.[29]
N/P-PC-1:5	H_3PO_4-N/P	130	2020	Qu et al.[16]
HCNFs-2	HNO_3-modified Hummers	143.6	2020	Gong et al.[17]
CK	KOH-HNO_3	142	–	This work

$$-COOH \rightarrow -COO + H^{+} + e^{-} \quad \text{(Equation 2)}$$

$$-C = O + e^{-} \rightarrow -C - O^{-} \quad \text{(Equation 3)}$$

Figure 4E displays the GCD profiles of CKN-2 at different current densities. It can be observed that the GCD curves of all samples exhibit a similar isosceles triangle shape with almost equal charge and discharge times, indicating good electrochemical reversibility of the material. The porous structure of CKN-2 can provide ion transport channels and electrolyte reservoirs, ensuring effective ion transport at high charge and discharge rates.[36]

It can be concluded from the aforementioned three-electrode system that the CKN-2 electrode material exhibits superior electrochemical properties after KOH-HNO_3 co-activation. To further investigate the practical application of CKN-2 electrode materials in supercapacitor, button symmetric (CKN-2//CKN-2) supercapacitors were assembled using CKN-2 materials and their electrochemical performance test results were shown in Figure 5.

Figure 5A shows the CV curves of the CKN-2//CKN-2 capacitors at different current densities. The curves are rectangular-like, indicating mainly the characteristics of double-layer capacitance. Figure 5B presents the GCD curves of the CKN-2//CKN-2 capacitors at different current densities, which exhibit an isosceles triangular shape, further confirming the double-layer capacitance behavior. The specific capacitance of the capacitor reaches 50 F/g at a current density of 0.5 A/g, as calculated from Equation 5. The high specific surface area provides a sufficient interface for the storage of electrolyte ions, while the porous, sparse, and layered structure ensures fast and efficient diffusion and transport of electrolyte ions. Figure 5C displays the EIS pattern of the CKN-2//CKN-2 capacitor, showing that the supercapacitor has low resistance, in agreement with the results for the three-electrode system. In the low-frequency region, the linear part of the impedance plot is close to 90°, indicating that the material exhibits typical bilayer capacitive behavior.

Figure 5D presents the specific capacitance of the CKN-2//CKN-2 capacitor at different current densities. The specific capacitance values at 0.5 A/g, 1 A/g, 2 A/g, 5 A/g, and 10 A/g current densities are 50 F/g, 47 F/g, 46 F/g, 45 F/g, and 42 F/g, respectively, indicating good multiplicative performance.[37] Figure 5E shows the Ragone plot of the CKN-2//CKN-2 capacitor. The energy density and power density of the capacitor can be calculated from Equations 6 and 7, respectively. The maximum energy density of the CKN-2 material is 6.80 Wh/kg at a power density of 244.8 W/kg Figure 5F displays the cycling performance graph of the CKN-2//CKN-2 capacitor's energy density, which indicates that the material achieves 97% capacitance retention after 10,000 cycles at 2 A/g current density, demonstrating high electrochemical stability and reversibility.

RESULTS AND DISCUSSION

In this work, CKN-2 prepared by KOH-HNO_3 sequential co-activation technique, exhibited excellent electrochemical properties due to its high specific surface area (625 m^2/g), large average pore size (4.690 nm), large mesopore volume (0.495 cm^3/g), high mesoporosity (83.193%), high surface oxygen-containing functional groups, and good wettability. The specific capacitance of CKN-2 obtained 142 F/g at a current density of 0.5 A/g in a three-electrode system. And then a symmetrical capacitor (CKN-2//CKN-2) was assembled using CKN-2 as active electrode materials. The energy density of CKN-2//CKN-2 was 6.80 Wh/Kg at a power density of 244.8 W/kg, and the capacitance retention rate of CKN-2//CKN-2 could still keep 97% after 10,000 cycles of charge and discharge tests. In summary, the low-temperature fire activation of KOH and the wet activation of HNO_3 can improve the electrochemical properties of the residual carbon from gasification slag. However, the KOH-HNO_3 co-activation offers the most effective approach to enhance the electrochemical properties of the residual carbon. The low-cost and high-yield nature of residual carbon from gasification slag, along with the potential for its activation and preparation as an electrode material for supercapacitors, can greatly reduce the cost of electrode materials compared to current carbon electrode materials. The KOH-HNO_3 co-activation approach can make a significant contribution to the "zero emission" of coal gasification and provide ideas for the high-value utilization of carbon-containing solid waste.

Limitations of the study

This work uses KOH and HNO3, which are strong acid and base reagents and require extra care during operation. If handled improperly or operated carelessly, it may cause harm to humans and the environment. Although KOH-HNO3 activation can change the chemical properties of the residual carbon from gasification fine slag, it is relatively difficult to modulate the microstructure. This may lead to an uneven distribution

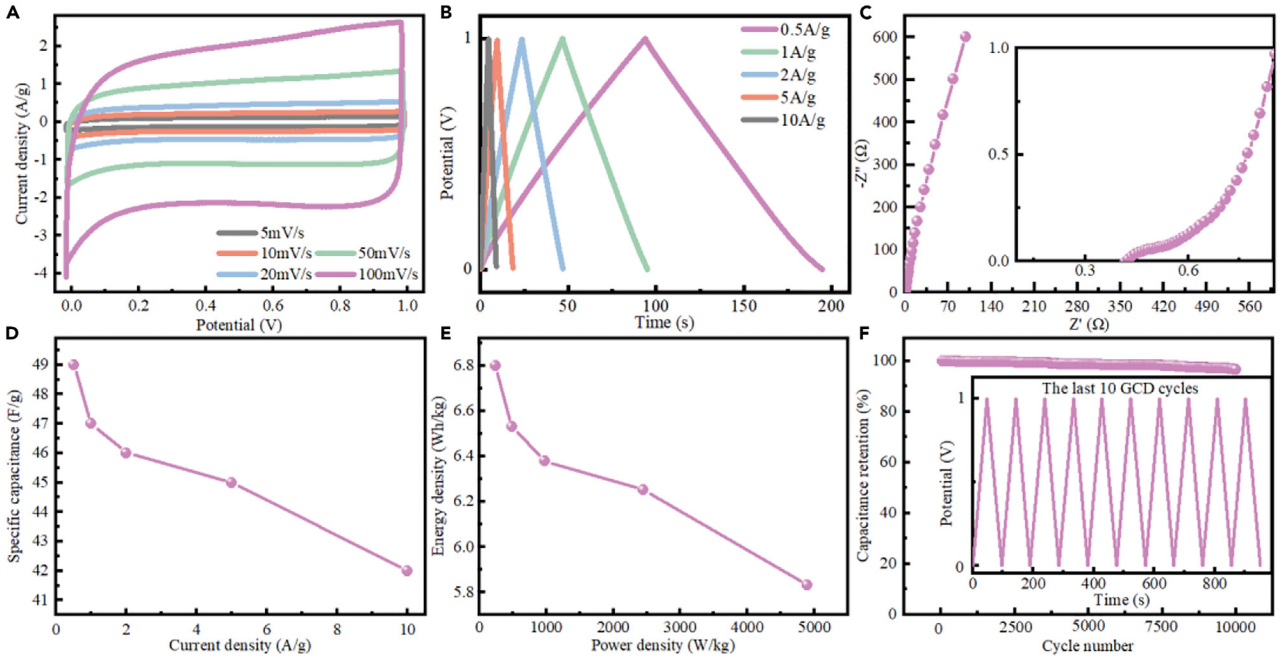

Figure 5. Supercapacitors testing

Electrochemical performances of CKN-2//CKN-2 capacitors: (A) CV curves at different scan rates, (B) GCD curves at different current densities, (C) EIS curves, (D) Multiplier performance, (E) Ragone pattern, (F) cycling stability.

of the pore structure and specific surface area of the electrode material, thus affecting the electrochemical performance. The treatment of waste liquids also requires specialized treatment methods. Treatment processes under highly acidic or alkaline conditions may pose environmental and safety challenges.

STAR★METHODS

Detailed methods are provided in the online version of this paper and include the following:

- KEY RESOURCES TABLE
- RESOURCE AVAILABILITY
  - Lead contact
  - Materials availability
  - Data and code availability
- METHOD DETAILS
  - Materials
  - Material characterization
  - Electrochemical characterization

ACKNOWLEDGMENTS

The authors appreciate the supports from the Resource utilization of carbon residue in caustic sludge and gasification slag (BDSD1-JS-2021-021), Key Special Project of "Science and Technology for Prosperity of Mongolia": Research on resource utilization of coal chemical solid waste (2021EEDSCXSFQZD008), the Fundamental Research Funds for Inner Mongolia University of Science & Technology (2023XKJX007), Program for Innovative Research Team in Universities of Inner Mongolia Autonomous Region, China (NMGIRT2215), and Major Project of Inner Mongolia (2020ZD17).

AUTHOR CONTRIBUTIONS

J. Z.: Conceptualization, validation, methodology, data curation, writing – original draft. J. S.: Conceptualization, funding acquisition, writing – review & editing, supervision. B. H.: Methodology, validation, data curation, investigation. J. G.: Writing – review & editing. Z. L.: Writing – review & editing. Y. W.: Writing – review & editing. G. X.: Writing – review & editing.

DECLARATION OF INTERESTS

The authors declare no competing interests.

Received: June 21, 2023
Revised: September 1, 2023
Accepted: October 9, 2023
Published: October 12, 2023

REFERENCES

1. Deng, W., Xu, Y., Zhang, X., Li, C., Liu, Y., Xiang, K., and Chen, H. (2022). $(NH_4)_2Co_2V_{10}O_{28}\cdot16H_2O/(NH_4)_2V_{10}O_{25}\cdot8H_2O$ heterostructure as cathode for high-performance aqueous Zn-ion batteries. J. Alloys Compd. *903*, 163824.
2. Deng, W.N., Li, Y.H., Xu, D.F., Zhou, W., Xiang, K.X., and Chen, H. (2022). Three-dimensional hierarchically porous nitrogen-doped carbon from water hyacinth as selenium host for high-performance lithium–selenium batteries. Rare Met. *41*, 3432–3445.
3. Wang, J., Yin, H., Wang, Z., Gao, J., Jiang, Q., Xu, Y., and Chen, Z. (2022). High performance Sn based anode with robust lignin derived hard carbon support for sodium ion batteries. Asia Pac. J. Chem. Eng. *17*, e2768.
4. Liu, C., Hou, Y., Li, Y., and Xiao, H. (2022). Heteroatom-doped porous carbon microspheres derived from ionic liquid-lignin solution for high performance supercapacitors. J. Colloid Interface Sci. *614*, 566–573.
5. Wang, L., Xie, L., Feng, X., Ma, H., Li, X., and Zhou, J. (2021). Sustainable lignin-derived hierarchical porous carbon for supercapacitors: a novel approach for holding electrochemical attraction natural texture property of precursor. ACS Omega *6*, 33171–33179.
6. Liu, S., Ren, Z., Fakudze, S., Shang, Q., Chen, J., Liu, C., Han, J., and Tian, Z. (2022). Structural evolution of graphitic carbon derived from ionic liquids-dissolved cellulose and its application as lithium-ion battery anodes. Langmuir *38*, 320–331.
7. Wen, X., Luo, J., Xiang, K., Zhou, W., Zhang, C., and Chen, H. (2023). High-performance monoclinic WO_3 nanospheres with the novel NH^{4+} diffusion behaviors for aqueous ammonium-ion batteries. Chem. Eng. J. *458*, 141381.
8. Akdemir, M. (2022). Electrochemical performance of Quercus infectoria as a supercapacitor carbon electrode material. Int. J. Energy Res. *46*, 7722–7731.
9. Awitdrus, A., Yusra, D.A., Taer, E., Agustino, A., Apriwandi, A., Farma, R., and Taslim, R. (2022). Biomass conversion into activated carbon as a sustainable energy material for the development of supercapacitor devices. Energy Sources, Part A Recovery, Util. Environ. Eff. *44*, 3349–3359.
10. Adan-Mas, A., Alcaraz, L., Arévalo-Cid, P., López-Gómez, F.A., and Montemor, F. (2021). Coffee-derived activated carbon from second biowaste for supercapacitor applications. Waste Manag. *120*, 280–289.
11. Shrestha, D., and Rajbhandari, A. (2021). The effects of different activating agents on the physical and electrochemical properties of activated carbon electrodes fabricated from wood-dust of Shorea robusta. Heliyon *7*, e07917.
12. Yaglikci, S., Gokce, Y., Yagmur, E., and Aktas, Z. (2020). The performance of sulphur doped activated carbon supercapacitors prepared from waste tea. Environ. Technol. *41*, 36–48.
13. Sharma, P., Singh, D., Minakshi, M., Quadsia, S., and Ahuja, R. (2022). Activation Induced surface modulation of Biowaste Derived hierarchical porous carbon for supercapacitors. Chempluschem *87*, e202200126.
14. Mahfoz, W., Shah, S.S., Aziz, M.A., and Al-Betar, A.R. (2022). Fabrication of high-performance supercapacitor using date leaves-derived submicron/nanocarbon. J. Saudi Chem. Soc. *26*, 101570.
15. Zhang, X., Zhao, M., Chen, Z., Yan, T., Li, J., Ma, Y., and Ma, L. (2022). The application of biomass-based carbon materials in flexible all-solid supercapacitors. J. Mater. Sci. Mater. Electron. *33*, 15422–15432.
16. Qu, Y., Liu, L., Li, L., Wen, S., Wei, D., Xiao, N., Yan, F., Yu, J., and Wang, L. (2020). Synthesis of nitrogen and phosphorus co-doped carbon with tunable hierarchical porous structure from rice husk for high performance supercapacitors. Int. J. Electrochem. Sci. *15*, 2399–2413.
17. Gong, Y., Zeng, X.G., Luo, T., Dai, Z.Y., Jin, Y.Z., Chen, J., and Tang, Y.J. (2020). Electric double-layer capacitance and pseudocapacitance contributions to the oxidative modification of helical carbon [J]. Int. J. Electrochem. Sci. *15*, 7508–7519.
18. Dat, N.T., Tran, T.T.V., Van, C.N., Vo, D.V.N., Kongparakul, S., Zhang, H., Guan, G., and Samart, C. (2020). Carbon sequestration through hydrothermal carbonization of expired fresh milk and its application in supercapacitor. Biomass Bioenergy *143*, 105836.
19. Dong, D., Zhang, Y., Xiao, Y., Wang, T., Wang, J., Romero, C.E., and Pan, W.P. (2020). High performance aqueous supercapacitor based on nitrogen-doped coal-based activated carbon electrode materials. J. Colloid Interface Sci. *580*, 77–87.
20. Zhao, H., Wang, L., Jia, D., Xia, W., Li, J., and Guo, Z. (2014). Coal based activated carbon nanofibers prepared by electrospinning. J. Mater. Chem. A *2*, 9338–9344.
21. Feng, L., Yan, B., Zheng, J., Zhang, Q., Wei, R., Zhang, C., Han, J., Jiang, S., and He, S. (2023). Chemical foaming-assisted synthesis of N, O co-doped hierarchical porous carbon from soybean protein for high rate performance supercapacitors. Diam. Relat. Mater. *133*, 109767.
22. Hao, E., Liu, W., Liu, S., Zhang, Y., Wang, H., Chen, S., Cheng, F., Zhao, S., and Yang, H. (2017). Rich sulfur doped porous carbon materials derived from ginkgo leaves for multiple electrochemical energy storage devices. J. Mater. Chem. A Mater. *5*, 2204–2214.
23. Xu, S., Zhou, Z., Gao, X., Yu, G., and Gong, X. (2009). The gasification reactivity of unburned carbon present in gasification slag from entrained-flow gasifier. Fuel Process. Technol. *90*, 1062–1070.
24. He, D., Niu, J., Dou, M., Ji, J., Huang, Y., and Wang, F. (2017). Nitrogen and oxygen co-doped carbon networks with a mesopore-dominant hierarchical porosity for high energy and power density supercapacitors. Electrochim. Acta *238*, 310–318.
25. Yan, B., Zheng, J., Feng, L., Zhang, Q., Zhang, C., Ding, Y., and He, S. (2023). Pore engineering: Structure-capacitance correlations for biomass-derived porous carbon materials. Mater. Des. *229*, 111904.
26. Liu, W., Mei, J., Liu, G., Kou, Q., Yi, T., and Xiao, S. (2018). Nitrogen-doped hierarchical porous carbon from wheat straw for supercapacitors. ACS Sustain. Chem. Eng. *6*, 11595–11605.
27. Thilageshwaran, S., Ansari, M.N.M., Nordin, N.A., Bassam, A., Yahya, Z., Elumalai, P., and Prasath, A. (2020). Electrochemical study on Activated Carbon Electrode from Kenaf biowaste for Supercapacitor Application. In 2020 International Conference and Utility Exhibition on Energy, Environment and Climate Change (ICUE) (IEEE), pp. 1–5.
28. Mandal, M., Subudhi, S., Alam, I., Subramanyam, B.V.R.S., Das, S., Raiguru, J., and Mahanandia, P. (2020). Effect of different aqueous electrolytes on electrochemical performance of activated carbon anchored by multiwalled carbon nanotubes for supercapacitor applications. AIP Conf. Proc. *2265*, 1.
29. Punon, M., Jarernboon, W., and Laokul, P. (2022). Electrochemical performance of Palmyra palm shell activated carbon prepared by carbonization followed by microwave reflux treatment. Mater. Res. Express *9*, 065603.
30. Lozano-Castelló, D., Calo, J.M., Cazorla-Amorós, D., and Linares-Solano, A. (2007). Carbon activation with KOH as explored by temperature programmed techniques, and the effects of hydrogen. Carbon *45*, 2529–2536.
31. Huang, J.Y., Li, S.H., Ge, M.Z., Wang, L.N., Xing, T.L., Chen, G.Q., Liu, X.F., Al-Deyab, S.S., Zhang, K.Q., Chen, T., and Lai, Y.K. (2015). Robust superhydrophobic TiO_2@ fabrics for UV shielding, self-cleaning and oil–water separation. J. Mater. Chem. A Mater. *3*, 2825–2832.
32. Zhou, B., Liu, W., Gong, Y., Dong, L., and Deng, Y. (2019). High-performance pseudocapacitors from kraft lignin modified active carbon. Electrochim. Acta *320*, 134640.
33. Zhao, W., Yan, B., Chen, D., Chen, J., Zhang, Q., Jiang, L., Lan, T., Zhang, C., Yang, W., and He, S. (2023). Free-standing carbon network with enhanced capacitive performance synthesized via green H_2O_2 activation. Colloids Surf. A Physicochem. Eng. Asp. *668*, 131425.

34. Gong, C., Wang, X., Ma, D., Chen, H., Zhang, S., and Liao, Z. (2016). Microporous carbon from a biological waste-stiff silkworm for capacitive energy storage. Electrochim. Acta *220*, 331–339.
35. Lu, Q., Zhou, S., Li, B., Wei, H., Zhang, D., Hu, J., Zhang, L., Zhang, J., and Liu, Q. (2020). Mesopore-rich carbon flakes derived from lotus leaves and it's ultrahigh performance for supercapacitors. Electrochim. Acta *333*, 135481.
36. Zhang, X., Zhao, M., Chen, Z., Yan, T., Li, J., Ma, Y., and Ma, L. (2022). The application of biomass-based carbon materials in flexible all-solid supercapacitors. J. Mater. Sci. Mater. Electron. *33*, 15422–15432.
37. Chen, Z., Chen, G., Wang, C., Chen, D., Zhang, Q., Jiang, L., Zhang, C., Liu, K., and He, S. (2023). Capacitive properties of carbon nanofibers derived from blends of cellulose acetate and polyacrylonitrile. New J. Chem. *47*, 13831–13840.
38. Wei, F., Zhang, H.F., He, X.J., Ma, H., Dong, S.A., and Xie, X.Y. (2019). Synthesis of porous carbons from coal tar pitch for high-performance supercapacitors. N. Carbon Mater. *34*, 132–139.
39. Karakaş, D.E., Akdemir, M., Kaya, M., Horoz, S., and Yaşar, F. (2022). The dual functionality of Zn@ BP catalyst: methanolysis and supercapatior. J. Mater. Sci. Mater. Electron. *33*, 13484–13492.
40. Peng, Z., Guo, Z., Chu, W., and Wei, M. (2016). Facile synthesis of high-surface-area activated carbon from coal for supercapacitors and high CO_2 sorption. RSC Adv. *6*, 42019–42028.

STAR★METHODS

KEY RESOURCES TABLE

REAGENT or RESOURCE	SOURCE	IDENTIFIER
Chemicals, peptides, and recombinant proteins		
KOH	Tianjin Beilian Fine Chemical Co.	HG3-952-76
residual Carbon from gasification fine slag	Inner Mongolia Bdsd Chemical Co, Ltd	N/A
HNO3	Tianjin Beilian Fine Chemical Co.	GB/T678-2002
Critical commercial assays		
XRD	Bruker AXS, Germany	D8 Advance X-ray diffractometer
BET	Mike's Instruments, USA	ASAP 2460 tester
RAMAN	HORIBA, France	LabRAM HR Evolution Raman spectrometer
XPS	Hermo Scientific, UK	ESCAL spectrometer
TG-DTG	NETZSCH, Germany	STA449 F3
WCA	Harco, Beijing, China.	HARKE-SPCA tester
electrochemical workstation	Shanghai Chenhua, China.	CHI660E

RESOURCE AVAILABILITY

Lead contact

Further information and requests for resources and reagents should be directed to and will be fulfilled by the lead contact, Jinling Song (sjl2010004@imust.edu.cn).

Materials availability

This study did not generate new unique reagents.

Data and code availability

- The paper does not report the original code.
- Any additional information required to reanalyze the data reported in this paper is available from the lead contact upon request.

METHOD DETAILS

Initially, 1.0 g of residual carbon (CK) obtained from gasification fine slag, which had passed through a 200 mesh sieve, was thoroughly mixed with KOH at a carbon-to-base mass ratio of 1:2. The resulting mixture was then transferred to a tube furnace, followed by feeding with N_2, and roasted at 500°C for 1.5 h. After cooling down to room temperature naturally, the sample was acid-washed with a mixture of 30 mL each of concentrated HCl, anhydrous ethanol, and deionized water for 6 h at 80°C. Subsequently, the sample was washed with water until it reached a neutral pH, and then dried for 6 h to obtain the alkali-activated sample (CK-2).

To obtain the acid-activated sample (CN-2), 1.0 g of CK was added to 100 mL of 2 mol/L HNO_3 solution, heated, and stirred at 80°C for 1 h. The resulting sample was then washed with water and dried.

To obtain the KOH-HNO_3 co-activated sample (CKN-2), the first two steps were repeated as outlined previously.

Materials

In this work, the reagents used were potassium hydroxide (KOH), concentrated nitric acid (HNO_3), concentrated hydrochloric acid (HCl), acetylene black (battery grade), polytetrafluoroethylene powder (PTFE), anhydrous ethanol (analytical purity) and nickel foam. All chemical reagents were used directly without any further pretreatment.

Material characterization

In this study, the content of each element was measured using X-ray fluorescence spectrometry (XRF). The phase composition of the samples was analyzed using X-ray diffraction (XRD) on a D8 Advance X-ray diffractometer manufactured by Bruker AXS in Germany. The specific surface area and pore volume of the samples were determined by N_2 adsorption-desorption isotherms and pore size analysis (BET) on an from

Mike's Instruments, USA. The graphitization and structural defects of the samples were evaluated using Raman spectroscopy (Raman) on a LabRAM HR Evolution Raman spectrometer from HORIBA, France. X-ray photoelectron spectroscopy (XPS) was conducted using an ESCAL spectrometer from Hermo Scientific, UK, to analyze the elemental content and existence form of the samples. Thermogravimetric analysis (TG-DTG) was performed with a synchronous thermal analyzer STA449 F3 from NETZSCH, Germany, to analyze the material's mass loss process under an air atmosphere and a temperature rise rate of 10°C/min. The surface morphology of the material was analyzed using scanning electron microscopy (SEM) with a Gemini SEM-300 microscope. The wettability of the material was characterized using a water contact angle (WCA) on a HARKE-SPCA tester manufactured by Harco, Beijing, China.

Electrochemical characterization

A slurry was prepared by mixing CK, CK-2, CN-2 and CKN-2 with acetylene black and PTFE in a mass ratio of 8:1:1, and was stirred for 6 h, in which the mass of the active material is around 1.2 mg. The resulting mixture was then applied onto pre-cut nickel sheets, dried, and tested for electrochemical properties using cyclic voltammetry (CV), galvanostatic charge/discharge (GCD), and electrochemical impedance spectroscopy (EIS). The diaphragm used in the battery is water-based. The electrochemical measurements were performed using a CHI660E electrochemical workstation manufactured by Shanghai Chenhua, China.

The electrochemical properties of the prepared samples were tested in a three-electrode system with a potential window of -1 to 0 V. The specific capacitance per unit mass of electrode material in the three-electrode system was calculated according to the following equation:[38]

$$C = \frac{I\Delta t}{m\Delta U} \quad \text{(Equation 4)}$$

where I is the current in A, Δt is the discharge time in s, ΔU is the potential difference in V and m is the mass of the active substance in g.

In the two-electrode system, the electrolyte is a 6 mol/L KOH solution with a potential window of 0 to 1 V. The specific capacitance per mass unit of electrode material in the two-electrode system is calculated by the following equation:[39]

$$C = \frac{2I\Delta t}{m\Delta U} \quad \text{(Equation 5)}$$

where I is the constant current constant in A, Δt is the discharge time in s, ΔU is the potential difference in V, and m is the mass of active material in the single electrode material in g.

The energy density (E) and power density (P) of the capacitor are calculated according to the following equations:[40]

$$E = \frac{1}{2} C\Delta U^2 \frac{1}{3.6} \quad \text{(Equation 6)}$$

$$P = \frac{3600E}{\Delta t} \quad \text{(Equation 7)}$$

where C is the mass-specific capacitance in F/g, Δt is the discharge time in s and ΔU is the potential difference in V.